Solar Energy Materials & Solar Cells 215 (2020) 110647

Contents lists available at ScienceDirect

Solar Energy Materials and Solar Cells

journal homepage: http://www.elsevier.com/locate/solmat

Amorphous tin-gallium oxide buffer layers in (Ag,Cu)(In,Ga)Se_2 solar cells

F. Larsson *, J. Keller, J. Olsson, O. Donzel-Gargand, N.M. Martin, M. Edoff, T. Törndahl

Department of Materials Science and Engineering, Solar Cell Technology, Uppsala University, Box 534, SE-75121 Uppsala, Sweden

ARTICLE INFO

Keywords:
CIGS
ACIGS
Buffer layers
Atomic layer deposition
Band gap engineering
Interfaces

ABSTRACT

Amorphous tin-gallium oxide (a-SGO) grown with atomic layer deposition was evaluated as a buffer layer in (Ag,Cu)(In,Ga)Se_2 thin-film solar cells in search for a new material that is compatible with a variety of absorber band gaps. Hard and soft X-ray photoelectron spectroscopy on absorber/a-SGO stacks combined with J–V characterization of solar cells that were fabricated, showed that the conduction band alignment at the absorber/a-SGO interface can be tuned by varying the cation composition and/or growth temperature. Here, the surface band gap was 1.1 eV for the absorber. However, optical band gap data for a-SGO indicate that a suitable conduction band alignment can most likely be achieved even for wider absorber band gaps relevant for tandem top cells. A best efficiency of 17.0% was achieved for (Ag,Cu)(In,Ga)Se_2/a-SGO devices, compared to $\eta = 18.6\%$ for the best corresponding CdS reference. Lower fill factor and open-circuit voltage values were responsible for lower cell efficiencies. The reduced fill factor is explained by a larger series resistance, seemingly related to interface properties, which are yet to be optimized. Some layer constellations resulted in degradation in fill factor during light soaking as well. This may partly be explained by light-induced changes in the electrical properties of a-SGO, according to analysis of Al/SGO/n-Si metal-oxide-semiconductor capacitors that were fabricated and characterized with J–V and C–V. Moreover, the introduction of a 1 nm thick Ga_2O_3 interlayer between the absorber and a-SGO improved the open-circuit voltage, which further indicates that the absorber/a-SGO interface can be improved.

1. Introduction

Thin film solar cells are attractive for photovoltaic power generation. Partly because of a potentially lowered production cost, but also due to the compatibility with flexible lightweight substrates and architectural integration. At present, solar cells based on Cu(In,Ga)$(S,Se)_2$ (CIGS) absorber layers exhibit the highest efficiencies among the commercial single-junction thin-film technologies, with a certified record of 23.4% for lab-scale cells [1]. A promising next step to increase the efficiency of thin-film solar cells even further is the development of multi-junction devices, i.e. tandem solar cells. Conversion efficiencies above 25% have already been demonstrated for four-terminal CIGS/Perovskite tandem cells [2].

The development of more advanced solar cell structures is depending on the availability of buffer layers (also called selective contacts) with suitable electronic band structures. More precisely, there is a demand for contact materials with variable band alignments, which allow for more flexibility in the band-structure engineering of the entire device.

Presently, a few different buffer layers with variable conduction band minimum (CBM) energies have been evaluated for use in CIGS-based solar cells [3]. The most commonly used have been Zn(O,S), $Zn_{1-x}Sn_xO_y$ and $Zn_{1-x}Mg_xO_y$. In previous studies, $Zn_{1-x}Sn_xO_y$ grown by atomic layer deposition (ALD) has shown significant efficiency improvement for wide band gap absorbers, such as $CuGaSe_2$ and Cu_2ZnSnS_4 [4–7]. However, one potential drawback of $Zn_{1-x}Sn_xO_y$ is that its band gap is sensitive to several ALD process parameters, such as growth temperature and flow conditions. This is possibly correlated with microstructural variations observed in these films [8].

Aiming to develop a new buffer-layer material with a highly variable band gap and new interface chemistry, we recently developed an ALD process for amorphous $Sn_{1-x}Ga_xO_y$ (a-SGO) [9]. The amorphous structure of a-SGO minimizes the risk of secondary phase formation and eliminates possible concerns about lattice matching with the CIGS surface planes. In addition, Ga_2O_3 has been suggested to form a beneficial interface to CIGS with a low density of interface defects [10]. It might be possible to exploit a similar chemical passivation effect in a-SGO. Furthermore, a-SGO belongs to a family of transparent semiconducting oxides of transition metals, where the CBM is often dominated by metal

* Corresponding author.
E-mail address: Fredrik.Larsson@angstrom.uu.se (F. Larsson).

https://doi.org/10.1016/j.solmat.2020.110647
Received 2 April 2020; Received in revised form 15 May 2020; Accepted 29 May 2020
Available online 18 June 2020

s-orbitals [11]. Because of this, the CBM energy is in theory determined by the cation ratio. In the case of a-SGO, the electron affinity (χ) is predicted to be variable in a wide range, where the reported values range from around 3.0 eV for Ga_2O_3 to around 4.5 eV for SnO_2 [12–14].

A similar approach has also been investigated by Koida et al. who evaluated sputtered a-$In_{1-x}Ga_xO_y$ and a-$Ga_{1-x}Al_xO_y$ as buffer layer materials [15].

In this study, we introduced ALD a-SGO as a buffer layer in RbF post-deposition treated (Ag,Cu)(In,Ga)Se_2 (ACIGS-RbF) solar cells and evaluated its potential as a new buffer layer material. Transmission electron microscopy techniques were used to assess the film conformality and compositional homogeneity of the a-SGO layers. Soft and hard X-ray photoelectron spectroscopy (XPS and HAXPES) was used to measure the valence band discontinuity between a-SGO and the absorber, which allowed for an estimation of the conduction band offset (CBO) after input from optical reflection-transmission (R–T) measurement data. The solar cell devices were mainly characterized by current-density–voltage (J–V) and quantum efficiency (QE) measurements. Here, we compared with conventional CdS reference devices. An absorber surface band gap appropriate for both buffer alternatives was selected. Lastly, the effect of light soaking on the electrical properties of a-SGO was investigated by fabricating Al/a-SGO/n-Si metal-oxide-semiconductor capacitor (MOS-CAP) structures, which were characterized by means of J–V and capacitance–voltage (C–V) measurements.

2. Experimental details

2.1. Solar cell device fabrication

The solar cell devices used in this study have a SLG/Mo/ACIGS-RbF/(a-SGO or CdS)/ZnO:Al/(metal grid) layer structure with a total area of 0.5 cm^2.

All ACIGS material used within each experimental series was produced in a single co-evaporation process at Solibro Research AB. The resulting films are 2.3 μm thick with an average composition of ([Ag]+[Cu])/([In]+[Ga]) = 0.85 (±0.01), [Ga]/([In]+[Ga]) = 0.28 (±0.01) and [Ag]/([Ag]+[Cu]) = 0.19, as determined by X-ray fluorescence spectrometry (XRF). The absorbers were graded in Ga towards the back contact with a near-surface composition of [Ga]/([In]+[Ga]) = 0.18 (±0.01), as shown by glow-discharge optical emission spectroscopy in the supplementary information. This composition corresponds to a near-surface band gap of around 1.1 eV. The samples were capped with a CdS layer immediately after the ACIGS-RbF deposition. This capping layer was etched off by immersion in HCl (2 M) for 30 s just before buffer-layer deposition. This use of a capping layer significantly improves the experimental repeatability by reducing surface deterioration during storage, which lasted up to three weeks. Moreover, residual RbF salts are dissolved in the etching step, which is necessary when combining ALD with alkali-fluoride PDT processes [16]. The resulting absorber surfaces were depleted in Cu and Ga, and enriched in and Rb, according to HAXPES and XPS measurements (data not shown), similarly as previously reported for non-etched ACIGS-RbF [17].

The a-SGO buffer layers were grown in an F-120 ALD system (ASM Microchemistry) using tetrakis(dimethylamino)tin(IV) [DMA_4Sn, $Sn((CH_3)_2N)_4$], tris(dimethylamino)gallium(III) [DMA_3Ga, $Ga((CH_3)_2N)_3$] and deionized water as precursors, using a recently published process [9]. Buffer layers were deposited at both 125 °C and 175 °C to evaluate the effect of deposition temperature (the thermal budget during window-layer processing has previously been found to be a critical parameter when using KF PDT [18]). For each deposition temperature, series of buffer layers were fabricated with different a-SGO cation compositions, where each composition was controlled by using a super-cycle approach with the pulse scheme [(DMA_4Sn or DMA_3Ga):N_2:H_2O:N_2] and where the ratio between the number of metal-precursor pulses in the super cycle (Sn:Ga) controls the film composition. The pulse time was 1 s for all pulses. The resulting cation ratio in the deposited films was determined by XRF calibrated with Rutherford backscattering spectrometry. As already mentioned, this process is expected to result in a-SGO buffer layers with different electron affinities. In addition, note that the deposition temperature has shown no significant effect on film composition, but can still affect the optical band gap and presumably the electron affinity [9]. In these series, the buffer layer thickness was fixed to 25–30 nm, which required around 125 ALD sub-cycles at 125 °C and around 350 sub-cycles at 175 °C. In addition, another series was fabricated where the a-SGO thickness was varied between 8 nm and 51 nm at a fixed deposition temperature of 125 °C. A Sn:Ga precursor ratio of 7:1 was used in this series that resulted in a cation composition of x = [Ga]/([Ga]+[Sn]) = 0.18 ± 0.01. The best ACIGS/a-SGO solar cells were obtained for 14 nm thick a-SGO buffer layers with x = 0.25, after further variation of the cation composition and film thickness of a-SGO layers deposited at 125 °C. Furthermore, the possibility of chemically passivating the ACIGS/a-SGO interface was explored by introducing an approximately 1 nm thick Ga_2O_3 between the absorber and buffer layer. The Ga_2O_3 layer was grown with 10 ALD cycles at 125 °C, using the a-SGO ALD process described above.

Reference devices with CdS buffer layers were also fabricated, using the Ångström Solar Center (ÅSC) baseline chemical bath deposition process where CdS is grown in a solution of cadmium acetate, thiourea and ammonia at 60 °C [19]. The same process was also used for the CdS capping layer mentioned above.

After buffer layer deposition, the devices were finalized according to the ÅSC baseline [19], with the exception that no intrinsic ZnO layer was included between the buffer layer and the doped ZnO, neither for the CdS buffer layer references nor for the devices with a-SGO buffer layers.

2.2. Material characterization

The film conformality and compositional homogeneity of the a-SGO buffer layers were evaluated by scanning transmission electron microscopy (STEM). A Titan Themis 200 (FEI) microscope was used, equipped with a SuperX energy dispersive spectrometer (EDS) detector. The sample lamellae were prepared with a focused Ga-ion beam using a Strata DB235 (FEI) focused ion beam system, applying the in-situ lift-out method [20]. The final polishing step employed a 50 pA ion beam current accelerated at 5 kV in combination with XeF_2 to prevent surface precipitates on the lamella. The EDS data was processed using Hyperspy [21].

Synchrotron-based XPS and HAXPES measurements were performed at the beamline I09 at Diamond Light Source (UK) to gain information about the valence band alignment between a-SGO and ACIGS. Two samples were analyzed: (i) an absorber coated with 15–20 nm $Sn_{0.67}Ga_{0.33}O_y$ deposited at 125 °C, and (ii) a bare absorber surface as reference. Note that the absorber surfaces were etched in HCl solution as previously described. The spectra were recorded using excitation energies of 1.1 keV (soft X-rays) and 7.05 keV (hard X-rays) employing a high-energy electron analyser (VG Scienta EW4000) at normal emission. Hard X-rays were monochromized by a Si(111) double-crystal monochromator and soft X-rays by a plane grating monochromator using collimated light. A pass energy of 200 eV and 100 eV was used for the hard and soft X-rays, respectively. A defocused beam, with a size of about 400 μm^2, was used to minimize radiation damage and no evidence of beam damage was observed.

R–T measurements were performed on 90–100 nm a-SGO films grown on fused quartz at 125 °C with a Lambda 900 spectrometer (PerkinElmer) equipped with an integrating sphere. The absorption coefficients for different a-SGO films were extracted using a method described by Hong [22], after which the optical band gap values were estimated by Tauc's method [23].

2.3. Photoelectrical solar cell characterization

Illuminated J–V and QE measurements on the solar cell devices were

performed at 25 °C in custom-built set-ups. A tungsten halogen lamp was used as light source in the J–V measurements. The light-intensity was calibrated after external QE (EQE) measurements, in order to compensate for the spectrum mismatch between the halogen lamp and the standard AM1.5G spectrum. The reported data are for 12 cells per sample, where severely shunted cells were excluded from the analysis. If not otherwise stated, the devices were light soaked for 3–4 days under an Osram Powerstar HQI-T 250W metal-halide lamp, during which the devices were unintentionally heated by the lamp to about 60 °C.

The internal QE (IQE) was estimated by correcting the measured EQE after optical reflection measurements on the finalized device. The minimum absorber band gap was extracted with the QE^2 method, where IQE^2 is plotted versus photon energy and the band gap value is obtained from the energy intercept in a linear regression of the absorption onset. This band gap value is here approximately equal to the near-surface band gap of the ACIGS absorber.

2.4. MOSCAP fabrication and characterization

Al/a-SGO/n-Si MOSCAP structures were fabricated with three different a-SGO thicknesses ($d = 13/26/39$ nm) with a fixed cation ratio of $x = 0.81 \pm 0.01$. The reason for choosing this cation ratio is to achieve as low χ as possible (high Ga) but still being able to discern potential effects caused by the presence of Sn. The a-SGO films were deposited at 125 °C on (111)-oriented n/n^{++}-type silicon epitaxial wafers doped with As. The doping concentration (N_D) is $5 \cdot 10^{15}$ cm^3 in the 6–7 μm epitaxial top layer. HF etching was used to remove the native silicon oxide prior to a-SGO growth. A similar light-soaking treatment as for the solar cell devices was then performed for half of the samples for each a-SGO thickness. Circular Al contacts with areas varied in the range 0.05–5 mm^2 were deposited using e-beam evaporation through a shadow mask.

Dark J–V and C–V characteristics of the MOSCAPs were measured with a HP 4142B Modular DC Source/Monitor and a HP 4280A 1 MHz capacitance meter, respectively. The gate voltage was applied to the metal contact and ground was connected to the bottom of the wafer via a liquid Ga–In contact. In the C–V measurements, an oscillating signal of 1 MHz with an amplitude of 30 mV was applied, while the DC gate voltage bias was repeatedly swept between −1 and +1 V. A parallel capacitance model was applied to extract the capacitance (and conductance).

3. Results and discussion

3.1. Material properties of a-SGO films grown on ACIGS

A high-angle annular dark field (HAADF) STEM image of a $Sn_{0.82}Ga_{0.18}O_y$ film grown at 125 °C on HCl-etched ACIGS-RbF is shown in Fig. 1a. It can be seen that the a-SGO film is conformal and uniform, as expected from a well-functioning ALD process.

Furthermore, an elemental analysis was performed using STEM EDS to evaluate the compositional homogeneity. The resulting composition maps are shown in Fig. 1b, where the concentrations of Sn, Ga and O are included. The maps do not show any signs of significant compositional gradients within the a-SGO layer nor any detectable compositional deviation in the region close to the ACIGS/a-SGO interface. However, it is not possible to exclude small compositional differences in the first nanometers of the film, as compared to bulk composition. In fact, some compositional variation during the beginning of the growth is probable to occur when growing a ternary oxide with ALD, in case the two different sub-cycles used exhibit different growth rates on the substrate. The main contrast within the a-SGO film is caused by noise in the measurement. Unfortunately, the counting statistics cannot be improved here without substantial risk of beam-induced damages.

3.2. Estimation of the conduction band offset at the ACIGS/a-SGO interface

In order to first determine the valence band offset (ΔE_V) at the ACIGS/a-SGO interface, HAXPES was performed on two samples: (i) an HCl-etched ACIGS-RbF absorber coated with 15–20 nm $Sn_{0.67}Ga_{0.33}O_y$ deposited at 125 °C, and (ii) a bare HCl-etched ACIGS-RbF absorber surface as reference, For the absorber reference sample, a photon energy of 1100 eV was used to record the spectra for the $In3d_{5/2}$ core level and the valence band. The collected spectra are shown in Fig. 2a–c. The energy scale is calibrated after the adventitious carbon 1s peak at 284.8 eV. The binding energy for $In3d_{5/2}$ was determined to be 445.0 eV, after fitting the spectrum with a minimum number of Voigt profiles after subtracting the Shirley background. The energy position of the valence band edge (E_V) relative to the Fermi level (E_F) was determined to be 0.8 eV, by performing a linear extrapolation of the onset of the valence band to the baseline (see Fig. 2c).

For the ACIGS/a-SGO sample, soft X-rays ($E = 1100$ eV) were first used to measure the $Sn3d_{5/2}$ core level and valence band edge position in the "bulk" of the a-SGO film (i.e. away from the heterojunction). Hard X-rays ($E = 7050$ eV) were used to probe core levels in ACIGS and SGO, respectively, near the heterojunction. These recorded spectra are also shown in Fig. 2a–c. The "bulk" binding energy value for $Sn3d_{5/2}$ was determined to be 486.7 eV, with a corresponding value for the valence band edge of 1.3 eV, by using the fitting procedure described for the reference sample. The binding energy of the core levels near the interface region is 443.9 eV and 486.2 eV for $In3d_{5/2}$ and $Sn3d_{5/2}$, respectively.

Kraut's method was then used to calculate ΔE_V according to Eq. (1) [24]. The resulting value of ΔE_V is −1.1 eV. The energy differences used for the calculation are schematically visualized in Fig. 2d. Note that only relative shifts between the core levels or with respect to the valence band are used for the calculation of ΔE_v, thus independent of the calibration method.

$$\Delta E_V = \left(E^{SGO}_{Sn3d_{5/2}} - E^{SGO}_{V}\right) - \left(E^{ACIGS}_{In3d_{5/2}} - E^{ACIGS}_{V}\right) - \left(E^{interface}_{Sn3d_{5/2}} - E^{interface}_{In3d_{5/2}}\right) \quad (1)$$

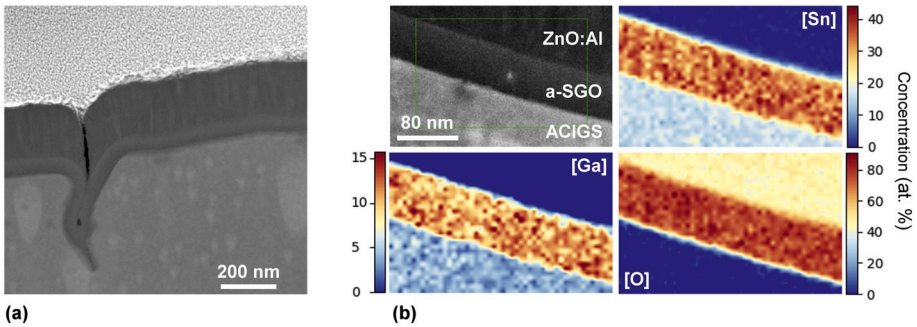

Fig. 1. (a) HAADF STEM cross-sectional image of a solar cell stack with a conformal and uniform $Sn_{0.82}Ga_{0.18}O_y$ film grown at 125 °C on HCl-etched ACIGS-RbF. (b) STEM EDS maps of Sn, Ga and O that show that the a-SGO layer is homogenous in composition.

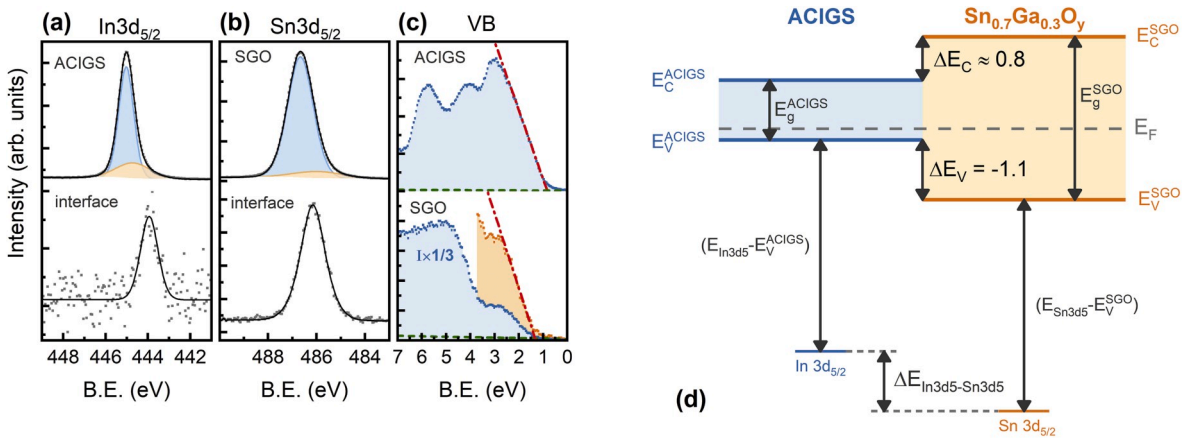

Fig. 2. (a)–(c) Raw and fitted soft and hard X-ray photoelectron spectroscopy spectra of the core levels ($In3d_{5/2}$and $Sn3d_{5/2}$) and valence band spectra used to calculate ΔE_V between HCl-etched ACIGS-RbF and $Sn_{0.67}Ga_{0.33}O_y$. The spectra denoted *ACIGS* and *SGO*, respectively, are recorded with 1100 eV X-rays and the spectra denoted *interface* were recorded with 7050 eV X-rays on an ACIGS/a-SGO stack. Note that the spectrum shown in (c) is presented with two different scales. (d) Schematic picture showing the measured energy values as well as the determined ΔE_V and estimated ΔE_C.

When ΔE_V is known, it is possible to get a first approximation of ΔE_C by adding the band gap difference to ΔE_V, according to Eq (2).

$$\Delta E_C \approx \Delta E_V + \left(E_g^{SGO} - E_g^{ACIGS}\right) \quad (2)$$

The optical band gap of the ACIGS surface was around 1.1 eV, as determined from QE measurements of ACIGS/SGO solar cell devices. The optical band gap was used for the a-SGO layer, which is around 3.0 eV for a $Sn_{0.77}Ga_{0.33}O_y$ film grown at 125 °C. For these band gap values, ΔE_C was estimated to be around 0.8 eV. This value corresponds to a moderately large spike in the conduction band and would likely produce a charge transport barrier at the ACIGS/a-SGO interface in a solar cell device [25]. It should be noted however, that the electronic band gaps for ACIGS and a-SGO are here assumed to be equivalent to the optical band gaps. It is also assumed that the band gap values are the same at the interface region as in the bulk of the materials. These assumptions may introduce some error in the absolute value of ΔE_C. Nevertheless, the HAXPES results indicate that a positive ΔE_C (commonly referred to as a spike-like CBO) can be achieved with a-SGO buffer layers on ACIGS-RbF absorbers.

3.3. Effect of a-SGO composition and ALD temperature on solar cell performance

In order to further investigate the effect of cation composition in a-SGO and to test the hypothesis that χ decreases with increased Ga content, two series of ACIGS/a-SGO solar cell devices with varying Ga content in the a-SGO buffer layers were fabricated and characterized, for two different ALD temperatures (T_{ALD}).

Fig. 3a and b shows J–V characteristics for the best devices where a-SGO buffer layers were grown at 125 °C and 175 °C and the cation ratio x in the buffer layers varied in the range 0–0.34 and 0–0.60, respectively. ACIGS/CdS devices are included as references. The J–V parameters V_{oc}, *FF*, J_{sc} and η are compared in Fig. 4.

In the series fabricated with T_{ALD} = 125 °C, the average V_{oc} value increased from 572 mV to 659 mV when x increased from 0 to 0.17. A further increase to x = 0.34 had a negligible effect on V_{oc}. An opposite trend was observed for *FF*. The average *FF* values were 58.4% and 60.0% for x = 0 and 0.17, respectively. When x was further increased to 0.34, the average *FF* value decreased to 48%. As seen in Fig. 3a, the *FF* drop is associated with an s-shaped J–V curve, which is characteristic for a charge transport barrier that is impeding both the photocurrent and forward current, e.g. due to a too high buffer layer CBM. The overall observation, with opposite trends in V_{oc} and *FF* values, are typical if the CBO at the absorber/buffer-layer interface is varied from a cliff-like to a spike-like offset. This is consistent with the band alignment estimations in section 3.1 that predicted that an a-SGO buffer layer with x = 0.33 grown at 125 °C would result in a too high CBO. This has been previously observed for other tunable buffer layers such as Zn(O,S) and $Zn_{1-x}Sn_xO_y$ [26,27]. The highest efficiencies were found for x = 0.17, where the average and best cell efficiency values are 13.6% and 14.6%, respectively. Therefore, a suitable CBO is likely found at, or slightly above, x = 0.17 for a-SGO buffer layers grown at 125 °C.

A similar trend can be observed for devices fabricated with T_{ALD} = 175 °C. However, there were a few differences. Firstly, devices with pure SnO_2 buffer layers (x = 0) resulted in significantly worse J–V

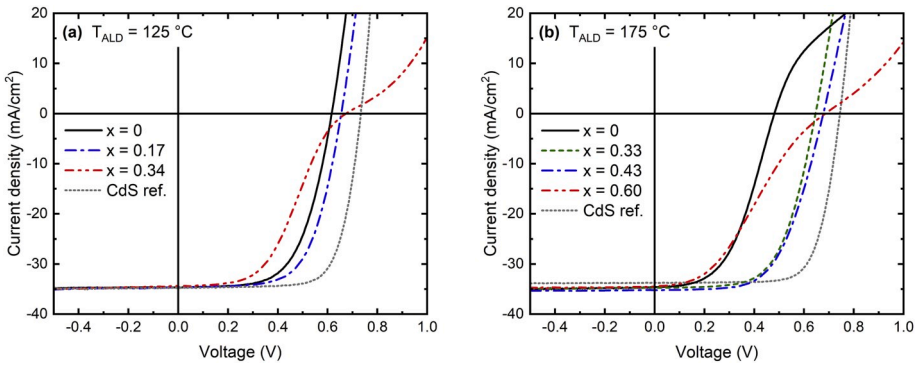

Fig. 3. Best-cell J–V characteristics for ACIGS/a-SGO devices where the cation ratio x was varied between (a) 0 and 0.34 for T_{ALD} = 125 °C, and (b) between 0 and 0.60 for T_{ALD} = 175 °C. The a-SGO thickness is 25–30 nm. ACIGS/CdS devices are included as reference.

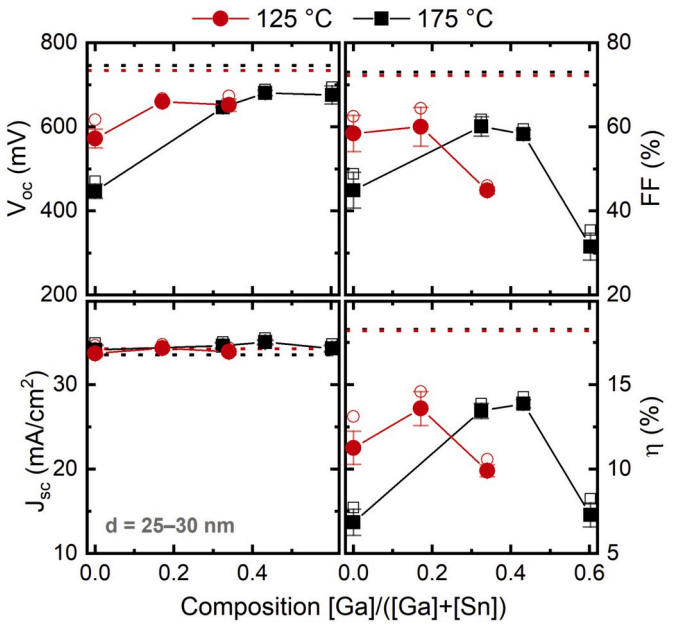

Fig. 4. Average (filled) and best (open) V_{oc}, *FF*, J_{sc} and η values for ACIGS/a-SGO devices where the cation composition was varied for T_{ALD} = 125 °C (red circles) and T_{ALD} = 175 °C (black squares). Dashed lines indicate the average value for ACIGS/CdS references. Error bars show the within-sample standard deviation. (For interpretation of the references to colour in this figure legend, the reader is referred to the Web version of this article.)

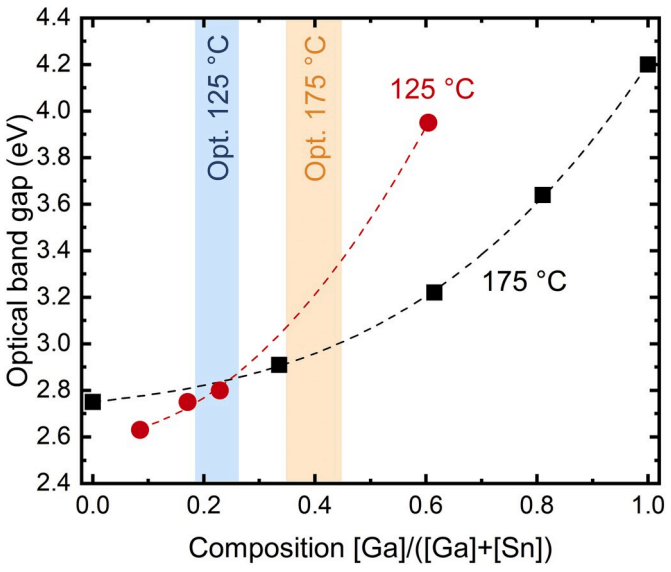

Fig. 5. Optical band gap of a-SGO for different cation composition values, determined by R–T measurements of 90–100 nm thick films grown on fused quartz. Values for T_{ALD} = 175 °C are taken from Ref. [9]. The filled backgrounds mark the optimal composition regions in terms of yielding the highest solar cell efficiency, for the ACIGS/a-SGO solar cells in this study, for each T_{ALD}.

characteristics for this ALD temperature. The average V_{oc} value was lower (446 mV compared to 572 mV for T_{ALD} = 125 °C) and the measured J–V curves exhibit a rollover behavior of unknown origin. Another difference is that the optimal composition was found at around $x = 0.4$ for $T_{ALD} = 175$ °C, as compared to $x = 0.2$ for $T_{ALD} = 125$ °C. The highest average and best efficiency values in this series were 13.9 and 14.3%, respectively, and were found for x = 0.43. Consequently, no evidence was found of an effect of T_{ALD} on the best cell efficiency. This indicates that the effects from the absorber surface modification induced by RbF PDT is stable for the ALD process temperature range in this study. In comparison, HCl-etched CIGS with KF PDT is very sensitive to the temperature used during window layer processing (including post-deposition annealing) [16,18].

The shift in optimal a-SGO composition suggests that χ varies with both cation ratio and the deposition temperature. This can be seen indirectly from how the optical band gap energy varies with cation composition for different T_{ALD}, which is shown in Fig. 5. It can be seen that the optimal compositions yield roughly the same optical band gap E_g = 2.8 ± 0.1 eV, but for different cation ratios. Note that it is not necessary that the band gaps are the same for the same electron affinity value. However, a major part of the band gap shift observed is likely explained by changes in electron affinity (as opposed to a lowered valence band position). It is therefore expected to be possible to tune the CBO even for absorbers with very wide band gap values, e.g. $CuGaSe_2$ or $Cu(Ga,In)S_2$.

The average efficiencies of the CdS references in these series were around 18.2–18.3%, which are significantly higher than for the devices with a-SGO buffer layers. The differences are in both higher *FF* and higher V_{oc} values for the CdS references as compared to the devices with a-SGO buffer layers.

3.4. Effect of a-SGO layer thickness on solar cell performance

Fig. 6 shows the average and best values for V_{oc}, *FF*, J_{sc} and η for a series of ACIGS/a-SGO devices where the thickness was varied (d = 8/26/51 nm) while the cation ratio was fixed to x = 0.18 ± 0.01. The

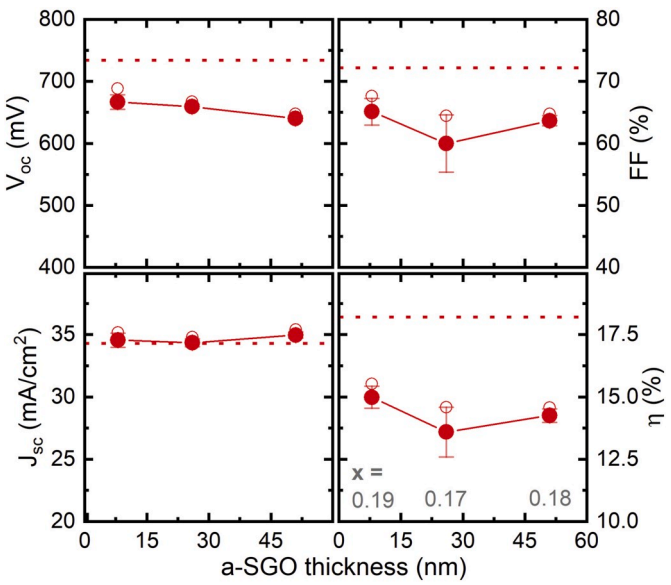

Fig. 6. Average (filled) and best (open) V_{oc}, *FF*, J_{sc} and η values for ACIGS/a-SGO devices where the a-SGO thickness varied for T_{ALD} = 125 °C. Dashed lines indicate the average value for an ACIGS/CdS reference. Error bars show the within-sample standard deviation.

dashed lines indicate the average values of the CdS reference devices. The sample with 8 nm a-SGO degraded during extended light soaking. Therefore, the values included in Fig. 6 for that sample correspond to 1 h of light soaking. The other two samples were light soaked until they reached a steady state (4 days), although the majority of the observed changes in J–V parameters from light soaking occur during the first 1–2 days (data not shown here). The J–V parameters for each sample, before and after light soaking, are listed in Table 1.

Interestingly, the best efficiency before light soaking was observed for the sample fabricated with an only 8 nm thick a-SGO layer. However, no major effects of a-SGO layer thickness on device performance could be identified. The average *FF* value for the sample with a 51 nm a-SGO

Table 1
Average (and best) J–V parameters for ACIGS/a-SGO devices with different a-SGO thicknesses. The a-SGO films were grown at 125 °C.

Buffer layer	LS	V_{oc} (mV)	FF (%)	J_{sc} (mA/cm^2)	η (%)
8 nm a-SGO (x = 0.19)	No LS	644 (673)	65.5 (67.4)	34.5 (35.1)	14.6 (15.1)
	1 h	667 (689)	65.1 (67.6)	34.6 (35.2)	15.0 (15.5)
	3 days	626 (659)	56.0 (64.7)	34.4 (35.7)	12.2 (15.0)
26 nm a-SGO (x = 0.17)	No LS	606 (623)	59.2 (63.7)	34.5 (35.1)	12.4 (13.7)
	4 days	660 (667)	60.0 (64.4)	34.4 (34.8)	13.6 (14.6)
51 nm a-SGO (x = 0.18)	No LS	600 (610)	59.7 (61.3)	34.0 (34.4)	12.2 (12.4)
	4 days	640 (647)	63.7 (64.7)	35.0 (35.4)	14.3 (14.6)
CdS reference	No LS	737 (741)	72.1 (73.3)	34.2 (34.5)	18.2 (18.6)
	3 days	734 (736)	72.2 (73.2)	34.3 (34.7)	18.2 (18.6)

Table 2
Average (and best) J–V parameters for ACIGS/$Sn_{0.75}Ga_{0.25}O_y$ devices with or without Ga_2O_3 interlayer for different light-soaking treatments. The a-SGO and Ga_2O_3 films were grown at 125 °C, using 128 and 10 ALD cycles, respectively. Data for the corresponding CdS reference are included.

Sample	LS	V_{oc} (mV)	*FF* (%)	J_{sc} (mA/cm^2)	*η* (%)
ACIGS/a-SGO	No LS	689 (694)	67.2 (68.8)	34.0 (34.4)	15.8 (16.3)
	4 h	702 (705)	68.7 (69.8)	34.1 (34.7)	16.4 (17.0)
	2 days	702 (708)	67.5 (68.9)	34.1 (34.6)	16.2 (16.5)
ACIGS/Ga_2O_3/a-SGO	No LS	720 (721)	66.9 (68.3)	34.2 (34.7)	16.5 (17.0)
	4 h	721 (722)	65.0 (66.8)	33.9 (34.5)	15.9 (16.6)
	2 days	716 (720)	61.8 (63.6)	33.8 (34.4)	15.0 (15.6)
CdS reference	No LS	737 (741)	72.1 (73.3)	34.2 (34.5)	18.2 (18.6)
	3 days	734 (736)	72.2 (73.2)	34.3 (34.7)	18.2 (18.6)

layer was not much different from the corresponding value for 8 nm a-SGO (63.7% compared to 65.1%). Therefore, series resistance associated with charge transport within the a-SGO bulk can be ruled out as the main factor explaining the overall low FF values for the a-SGO devices. Such an effect would be distinctly thickness dependent.

3.5. Evaluation of best ACIGS/a-SGO solar cells in study

After further variations of the cation composition and film thickness of a-SGO layers deposited at 125 °C (not shown here), the best ACIGS/a-SGO device in this study was fabricated with a 14 nm thick a-SGO layer with a cation ratio of x = 0.25. The J–V characteristic of the best device is shown in Fig. 7a, compared to the best CdS reference device. Furthermore, average and best values of the extracted J–V parameters are listed in Table 2 for different light-soaking treatments.

The best cell efficiency was 17.0% after 4 h of light soaking, which can be compared to 18.6% of the best CdS reference device. However, this sample also showed slight degradation during extended light soaking, during which the efficiency stabilized at 16.5% after 2 days. As seen in Table 2, the change in efficiency is mainly accounted for by decreased *FF*.

The best a-SGO cell exhibited a *FF* of 69.8%, which is considerably lower than the *FF* of 73% obtained for the CdS reference. In order to investigate the underlying cause of this, a simple one-diode model was fitted to the J–V curves of the best devices with a-SGO and CdS, respectively. The fitted curves are shown in Fig. 7a, together with the extracted model parameters. The experimental data were well described by a single diode, and the diode ideality factor (A) and series-resistance (R_s) could be estimated. The resulting values for the diode ideality factor (A) and series resistance (R_s) are $A = 2.1$ and $R_s = 1.1$ Ωcm^2 for the device with a-SGO and $A = 2.0$ and $R_s = 0.65$ Ωcm^2 for the CdS reference. A high diode ideality factor of A ≈ 2 can indicate predominant Shockley–Read–Hall recombination through deep defects in the space charge region. The extracted ideality factor could also be affected by other non-ideal effects that are not included in the one-diode model, e.g. voltage-dependent current collection. However, the presence of any such possible effect can likely be neglected in this analysis, considering how well the model could describe the experimental data. If the *FF* values are corrected for series resistance (i.e. R_s set to zero in the one-diode model), a *FF* of 74% is obtained for the a-SGO device compared to 75% for the CdS reference. This suggests that the *FF* is limited by a higher series resistance in the ACIGS/a-SGO device. As previously discussed in section 3.4, this resistance is unlikely related to charge transport within the a-SGO layer. However, it may instead be associated with an impeded charge transport across the ACIGS/a-SGO or a-SGO/ZnO:Al interface.

The V_{oc} value was around 30 mV lower for the best a-SGO device compared to the best CdS reference. This is presumably caused by an

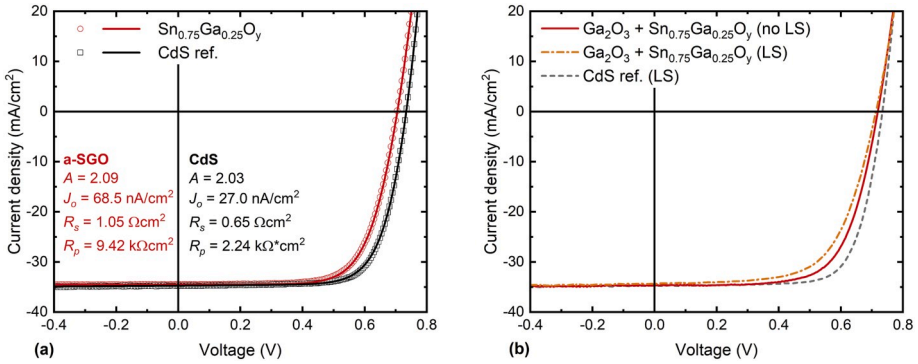

Fig. 7. (a) Fitted one-diode models (solid lines) and raw J–V data (open symbols) for the best ACIGS/a-SGO device and ACIGS/CdS reference after light soaking. (b) Best cell J–V characteristics for ACIGS/Ga_2O_3/a-SGO before and after light soaking, and the corresponding ACIGS/CdS reference after light soaking. The a-SGO and Ga_2O_3 films were grown at 125 °C, using 128 and 10 ALD cycles, respectively.

increased (near)-interface recombination rate, which can be affected by various factors in general (e.g. CBO, interface-defect density, and degree of band bending at the ACIGS surface).

The potential possibility to decrease the V_{oc} difference by chemically passivating the ACIGS/a-SGO interface was explored by adding a thin layer of Ga_2O_3 between the absorber and the buffer layer. Fig. 7b and Table 2 include such a device where 10 ALD cycles of Ga_2O_3 were deposited prior to a-SGO growth, which corresponds to approximately 1 nm of Ga_2O_3. With this structure, the V_{oc} difference could be reduced to 16–20 mV and a best cell efficiency of 17.0% was attained prior to light soaking. However, devices fabricated with this structure degraded during light soaking resulting in decreased *FF*, similar to the devices with thin a-SGO buffer layers. Despite of this, the relatively high V_{oc} values indicate that structures with a-SGO buffer layers can achieve relatively low (near)-interface recombination rates. Furthermore, the a-SGO layer is highly resistive and the (non-intentional) doping concentration has previously been estimated to be lower than 10^{13}–10^{15} cm^{-3} [9]. This suggests that the doping concentration in the buffer layer is not necessarily a crucial parameter when designing new buffer layer materials, in comparison to factors as CBO and interface-defect density. Note that the transparent conducting oxide layer is assumed to partake in the formation of the p–n junction in this case.

An important feature of a-SGO buffer layers is the improved transparency as compared to CdS due to a wider band gap, which reduces the parasitic absorption of photons with wavelengths below 550 nm. This can be seen in Fig. 8, where the IQE spectra (estimated by reflection-corrected EQE) are shown for the best devices with a-SGO and CdS buffer layers, respectively. Here, the IQE difference corresponds to a 1.7 mA/cm^2 difference in short-circuit current, assuming the AM1.5G spectrum and one-sun illumination. It should be noted that this difference could most likely be reduced by using a thinner CdS layer. However, the actual J_{sc} values calculated from the EQE spectra (included in Fig. 8 as dashed lines) are 35.4 mA/cm^2 and 35.1 mA/cm^2 for devices with a-SGO and CdS, respectively. Thus, the difference in $J_{sc,EQE}$ is only 0.3 mA/cm^2 as compared to the 1.7 mA/cm^2 contribution from parasitic absorption. This is mainly due to the position of the reflection fringes in relation to the AM1.5G spectrum. Note that the $J_{sc,EQE}$ values were used to calibrate J_{sc} for the J–V measurements. This means that the measured efficiencies of a-SGO and CdS reference devices are biased in favor of the CdS references.

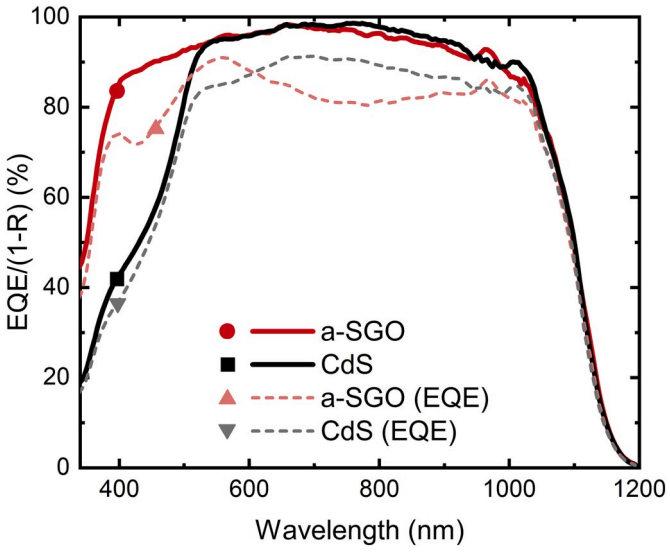

Fig. 8. Reflection-corrected EQE (solid lines) and EQE for the best ACIGS/a-SGO structure and the CdS reference, showing a reduced parasitic absorption for the a-SGO device.

3.6. *Effect of light soaking on electrical properties of a-SGO*

Pinpointing the exact mechanism behind the light-induced degradation of the a-SGO containing devices is challenging, considering the multitude of factors that can potentially affect the long-term and short-term stability of CIGS solar cells [28,29]. Furthermore, any possible light-soaking effect on the buffer-layer properties are superimposed on the known potential light-soaking effect on ACIGS bulk properties [30]. Instead, we simplify the question to whether or not the electrical properties of a-SGO itself are affected by light soaking, and if this can explain the observed FF degradation.

In an attempt to study effects of light soaking on a-SGO properties in isolation, Al/a-SGO/n-Si MOSCAP structures were fabricated and characterized with dark J–V and C–V. The MOSCAP layer structure is shown in Fig. 9a. Below, the main results are discussed for MOSCAPs fabricated with three different oxide thicknesses ($d = 13/26/39$ nm) with a cation ratio of $x = 0.81 \pm 0.01$. More extensive data are provided in supplementary information.

J–V characteristics of MOSCAPs with 26 nm a-SGO are shown in Fig. 9b, before and after 3 days light soaking. Both forward and reverse current are suppressed after light soaking, which may be interpreted as an increased charge-transport barrier. This was also observed for the sample with 13 nm a-SGO, but not for the one with 39 nm a-SGO. It is uncertain how this would translate into behavior of solar cell devices. However, it is noteworthy similar to the case for thickness series discussed in section 3.4, where only solar cell devices fabricated with thin a-SGO layers showed decreased *FF* values after light-soaking. In any case, this result alone shows that the properties of a-SGO can be affected by light treatments.

High-frequency C–V measurements were performed on all MOSCAPs at a frequency of 1 MHz. Simulated ideal C–V curves were fitted to the experimental data, with the relative dielectric constant of a-SGO (ε_{ox}) and fixed oxide charge (Q_f) as fitting parameters. As described in the supplementary information, ε_{ox} (together with oxide thickness) determines the higher capacitance limit (which is C_{ox}) while Q_f produces a shift in the so-called flat-band potential, which shifts the entire C–V curve along the voltage axis. The fixed inputs were a-SGO layer thickness, n-Si doping concentration (N_D) and the work-function difference between Al and n-Si (ϕ_{ms}). N_D was $5 \cdot 10^{15}$ cm^{-3} and ϕ_{ms} was assumed to be -0.17 eV. N_D mainly accounts for the lower capacitance limit. However, ϕ_{ms} also produces a shift in the flat-band potential, and thus causes an uncertainty in Q_f. To account for this, additional simulations were performed where ϕ_{ms} was varied within a range corresponding to its spread in literature values (the spread of Al work-function values in practice). Note that a good precision in the shift for Q_f after light soaking could be attained, regardless of the uncertainty in the absolute value of Q_f.

Fig. 9c shows a fitted C–V curve and the corresponding experimental data for a MOSCAP with 26 nm a-SGO. Here, the gate voltage was swept in reverse from +1 to −1 V. The faded data points are for similar devices from the same batch, and provide a rough measure of variation. Simulated curves could be very well fitted to the experimental data, and no interface trap states had to be included in the model, which would otherwise smear out the C–V curve [31]. This enabled the extraction of ε_{ox} and Q_f with high precision. The extracted values for ε_{ox} and shift in Q_f after light soaking are presented in Table 3.

The ε_{ox} values varied between devices with different a-SGO thicknesses, but seemed unaffected by light soaking. These values should however be considered as lower limits of the true ε_{ox}, as these are influenced by any native oxide layer and parasitic series resistance during the C–V measurements.

More interestingly, shifts in Q_f toward more positive charges were observed for the two samples with thinner a-SGO layers, and the largest shift was observed for 13 nm a-SGO. This may be an indication that the defect chemistry in the a-SGO layer is sensitive to illumination. Furthermore, a change in Q_f in solar cell structures can potentially affect

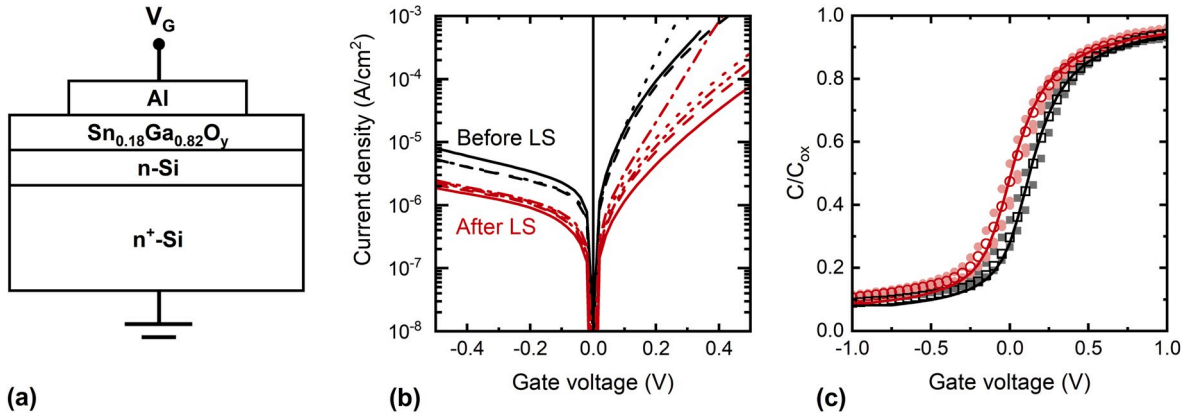

Fig. 9. (a) Schematic layer structure of Al/a-SGO/n-Si MOSCAPs. (b) Dark J–V characteristics of MOSCAPs with 26 nm a-SGO, before (black) and after (red) 3 days light soaking. (c) Fitted curves and raw data for high frequency (1 MHz) C–V measurement on MOSCAPs with 26 nm a-SGO, before (black, squares) and after (red, circles) light soaking. The faded data points are for other devices fabricated in the same batch. (For interpretation of the references to colour in this figure legend, the reader is referred to the Web version of this article.)

Table 3
Extracted values (and standard error) of ε_{ox} and shift in Q_f due to light soaking, obtained from fitted C–V curves for Al/a-SGO/n-Si MOSCAPs with different a-SGO thicknesses.

a-SGO thickness	ε_{ox}	$\varepsilon_{ox,\ LS}$	ΔQ_f (LS) [$\times 10^{11}$ cm^{-2}]
13 nm	5.9 ± 0.3	5.0 ± 0.3	4.2 ± 1.3
26 nm	7.6 ± 0.4	7.6 ± 0.1	1.7 ± 0.5
39 nm	6.5 ± 0.3	6.6 ± 0.6	0.1 ± 0.5

the properties of the absorber/buffer junction through altered band bending. However, this charge cannot explain the MOSCAPs J–V behavior, since a more positive net-charge in the oxide layer would rather facilitate than block forward-current transport (added positive charge is the same as added positive gate voltage [31]).

All a-SGO films appeared to exhibit negative fixed-oxide charge prior to light soaking, with an absolute Q_f value in the order of magnitude 10^{11} cm^{-2}, depending on the value assumed for the work-function of aluminum. See supplementary information for further details. In addition, some of the MOSCAPs showed a slight hysteresis effect that may indicate the presence of oxide trap states corresponding to a charge of up to around $1 \cdot 10^{11}$ cm^{-2}.

From the current J–V and C–V data, it is not possible to determine the mechanism behind the observations. One hypothesis is that negative charges in a-SGO are injected when current is flowing through the layer, and that light soaking affects the amount of injection by altering the current path through the layer (e.g. by inactivating current transport through sub-gap states). Regardless of the exact mechanism, it is shown that the electrical properties a-SGO are affected by light soaking, which is presumably the origin of the observed light-soaking effects on ACIGS/a-SGO solar cell devices.

4. Conclusions

Conformal and homogeneous a-SGO buffer layers were successfully grown on ACIGS absorber surfaces by ALD. It was confirmed that CBO (and indirectly χ) can be tuned by varying the [Ga]/([Ga]+[Sn]) cation ratio. Furthermore, it was shown that a suitable CBO can be achieved for different ALD temperatures (125 °C and 175 °C), making the ALD process more flexible compared to ALD of $Zn_{1-x}Sn_xO_y$.

A best cell efficiency of 17.0% was achieved for ACIGS/a-SGO devices as compared to 18.6% for the best ACIGS/CdS device. By replacing CdS with a-SGO, a clear reduction of parasitic absorption is achieved. However, all ACIGS/a-SGO devices exhibited lower V_{oc} and *FF* values as compared to the CdS references. The V_{oc} was roughly 30 mV lower for the best a-SGO device. This deficit could be reduced to around 16–20 mV by introducing a thin Ga_2O_3 interlayer between ACIGS and a-SGO. The *FF* difference was 3% absolute and accounted for the majority of the reduction in efficiency. J–V data indicated that this difference was mainly due to a higher series resistance value for the a-SGO device. Moreover, it appears to be associated with the ACIGS/a-SGO or a-SGO/ZnO:Al interface and not the a-SGO bulk properties, since no effect of a-SGO thickness on *FF* was observed.

Light-induced degradation was observed for some layer configurations. In particular, *FF* values were decreased after light soaking for devices with thin a-SGO layers ($d < 20$ nm) or for devices where a thin Ga_2O_3 interlayer was applied. J–V and C–V characterization of Al/$Sn_{0.19}Ga_{0.81}O_y$/n-Si MOSCAPs showed that the electrical properties of a-SGO are affected by light-soaking treatments and increased charge transport barriers were observed for thin a-SGO layers ($d = 13$ and 26 nm). In addition, the fixed-oxide charge was shifted to less negative values in these devices. It is uncertain how these effects translate into solar cell properties. In either case, the light-induced effects observed on the electrical properties of a-SGO may be responsible for the light-induced degradation of some ACIGS/a-SGO solar cells.

Lastly, we conclude that in order to improve the efficiency of ACIGS/a-SGO solar cells further, it is necessary to minimize the interface-related series resistance that currently seems to be the major limiting factor. Specifically the absorber/a-SGO and a-SGO/ZnO:Al interfaces need to be optimized and studied in more detail. Moreover, we predict that a-SGO can potentially be a suitable buffer layer for wide band gap absorbers, due to its flexible band gap and decent performance on narrow band gap ACIGS.

Declaration of competing interest

The authors declare that they have no known competing financial interests or personal relationships that could have appeared to influence the work reported in this paper.

CRediT authorship contribution statement

F. Larsson: Conceptualization, Investigation, Visualization, Writing - original draft. **J. Keller:** Investigation, Software, Supervision, Writing - review & editing. **J. Olsson:** Resources, Supervision, Writing - review & editing. **O. Donzel-Gargand:** Investigation, Writing - review & editing. **N.M. Martin:** Investigation, Resources, Writing - review & editing. **M. Edoff:** Resources, Supervision, Writing - review & editing. **T. Törndahl:** Conceptualization, Supervision, Funding acquisition, Writing - review & editing.

Acknowledgements

Financial support from the Swedish Energy Agency (grant no. 2017–004796) is gratefully acknowledged. The authors are also grateful for the ACIGS material provided by Solibro Research AB. Parts of this research were conducted at Diamond Light Source. We acknowledge Diamond Light Source for time on Beamline I09 under Proposal SI21742. Support from Dr. Pardeep Kumar at the Beamline is also acknowledged.

Appendix A. Supplementary data

Supplementary data related to this article can be found at https://doi.org/10.1016/j.solmat.2020.110647.

References

[1] M. Nakamura, K. Yamaguchi, Y. Kimoto, Y. Yasaki, T. Kato, H. Sugimoto, Cd-free Cu(in,Ga)(Se,S)$_2$ thin-film solar cell with record efficiency of 23.35%, IEEE J. Photovoltaics 9 (2019) 1863–1867, https://doi.org/10.1109/JPHOTOV.2019.2937218.

[2] D.H. Kim, C.P. Muzzillo, J. Tong, A.F. Palmstrom, B.W. Larson, C. Choi, S. P. Harvey, S. Glynn, J.B. Whitaker, F. Zhang, Z. Li, H. Lu, M.F.A.M. van Hest, J. J. Berry, L.M. Mansfield, Y. Huang, Y. Yan, K. Zhu, Bimolecular additives improve wide-band-gap perovskites for efficient tandem solar cells with CIGS, Joule 3 (2019) 1734–1745, https://doi.org/10.1016/j.joule.2019.04.012.

[3] W. Witte, S. Spiering, D. Hariskos, Substitution of the CdS buffer layer in CIGS thin-film solar cells: status of current research and record cell efficiencies, Vakuum Forsch. Praxis 26 (2014) 23–27, https://doi.org/10.1002/vipr.201400546.

[4] F. Larsson, N.S. Nilsson, J. Keller, C. Frisk, V. Kosyak, M. Edoff, T. Törndahl, Record 1.0 V open-circuit voltage in wide band gap chalcopyrite solar cells, Prog. Photovoltaics Res. Appl. 25 (2017) 755–763, https://doi.org/10.1002/pip.2914.

[5] C. Platzer-Björkman, C. Frisk, J.K. Larsen, T. Ericson, S.-Y. Li, J.J.S. Scragg, J. Keller, F. Larsson, T. Törndahl, Reduced interface recombination in Cu_2ZnSnS_4 solar cells with atomic layer deposition $Zn_{1-x}Sn_xO_y$ buffer layers, Appl. Phys. Lett. 107 (2015) 243904, https://doi.org/10.1063/1.4937998.

[6] T. Ericson, F. Larsson, T. Törndahl, C. Frisk, J. Larsen, V. Kosyak, C. Hägglund, S. Li, C. Platzer-Björkman, Zinc-tin-oxide buffer layer and low temperature post annealing resulting in a 9.0% efficient Cd-free Cu_2ZnSnS_4 solar cell, Sol. RRL. 1 (2017) 1700001, https://doi.org/10.1002/solr.201700001.

[7] J.K. Larsen, F. Larsson, T. Törndahl, N. Saini, L. Riekehr, Y. Ren, A. Biswal, D. Hauschild, L. Weinhardt, C. Heske, C. Platzer-Björkman, Cadmium free Cu_2ZnSnS_4 solar cells with 9.7% efficiency, Adv. Energy Mater. 9 (2019) 1900439, https://doi.org/10.1002/aenm.201900439.

[8] J. Lindahl, C. Hägglund, J.T. Wätjen, M. Edoff, T. Törndahl, The effect of substrate temperature on atomic layer deposited zinc tin oxide, Thin Solid Films 586 (2015) 82–87, https://doi.org/10.1016/j.tsf.2015.04.029.

[9] F. Larsson, J. Keller, D. Primetzhofer, L. Riekehr, M. Edoff, T. Törndahl, Atomic layer deposition of amorphous tin-gallium oxide films, J. Vac. Sci. Technol. 37 (2019), 030906, https://doi.org/10.1116/1.5092877.

[10] S. Garud, N. Gampa, T.G. Allen, R. Kotipalli, D. Flandre, M. Batuk, J. Hadermann, M. Meuris, J. Poortmans, A. Smets, B. Vermang, Surface passivation of CIGS solar cells using gallium oxide, Phys. Status Solidi 215 (2018) 1700826, https://doi.org/10.1002/pssa.201700826.

[11] T. Kamiya, H. Hosono, Material characteristics and applications of transparent amorphous oxide semiconductors, NPG Asia Mater. 2 (2010) 15–22, https://doi.org/10.1038/asiamat.2010.5.

[12] M.N. Islam, M.O. Hakim, Electron affinity and work function of polycrystalline SnO2 thin film, J. Mater. Sci. Lett. 5 (1986) 63–65, https://doi.org/10.1007/BF01671438.

[13] W. Guo, Y. Guo, H. Dong, X. Zhou, Tailoring the electronic structure of β-Ga_2O_3 by non-metal doping from hybrid density functional theory calculations, Phys. Chem. Chem. Phys. 17 (2015) 5817–5825, https://doi.org/10.1039/C4CP05637J.

[14] H. Park, J.H. Choi, K.M. Choi, D.K. Lee, J.K. Kang, Highly porous gallium oxide with a high CO_2 affinity for the photocatalytic conversion of carbon dioxide into methane, J. Mater. Chem. 22 (2012) 5304, https://doi.org/10.1039/c2jm30337j.

[15] T. Koida, Y. Kamikawa-Shimizu, A. Yamada, H. Shibata, S. Niki, Cu(In,Ga)Se_2 solar cells with amorphous oxide semiconducting buffer layers, IEEE Journal of Photovoltaics 5 (2015) 956–961, https://doi.org/10.1109/JPHOTOV.2015.2396356.

[16] F. Larsson, O. Donzel-Gargand, J. Keller, M. Edoff, T. Törndahl, Atomic layer deposition of Zn(O,S) buffer layers for Cu(In,Ga)Se_2 solar cells with KF post-deposition treatment, Sol. Energy Mater. Sol. Cell. 183 (2018) 8–15, https://doi.org/10.1016/j.solmat.2018.03.045.

[17] M. Edoff, T. Torndahl, F. Larsson, O. Stolt, N. Shariati Nilsson, L. Stolt, Post deposition treatments of (Ag,Cu)(In,Ga)Se_2 thin films for solar cells. IEEE 46th Photovoltaic Specialists Conference (PVSC), IEEE, Chicago, IL, USA, 2019, pp. 618–621, https://doi.org/10.1109/PVSC40753.2019.8981287, 2019.

[18] J. Keller, F. Chalvet, J. Joel, A. Aijaz, T. Kubart, L. Riekehr, M. Edoff, L. Stolt, T. Törndahl, Effect of KF absorber treatment on the functionality of different transparent conductive oxide layers in CIGSe solar cells. Progress in Photovoltaics: Research and Applications, 2017, https://doi.org/10.1002/pip.2925.

[19] J. Lindahl, U. Zimmermann, P. Szaniawski, T. Torndahl, A. Hultqvist, P. Salome, C. Platzer-Bjorkman, M. Edoff, Inline Cu(in,Ga)Se_2 Co-evaporation for high-efficiency solar cells and modules, IEEE Journal of Photovoltaics 3 (2013) 1100–1105, https://doi.org/10.1109/JPHOTOV.2013.2256232.

[20] R.M. Langford, M. Rogers, In situ lift-out: steps to improve yield and a comparison with other FIB TEM sample preparation techniques, Micron 39 (2008) 1325–1330, https://doi.org/10.1016/j.micron.2008.02.006.

[21] Francisco de la Peña, Eric Prestat, Vidar Tonaas Fauske, Pierre Burdet, Petras Jokubauskas, Magnus Nord, Tomas Ostasevicius, Katherine E. MacArthur, Mike Sarahan, Duncan N. Johnstone, Joshua Taillon, Lähnemann Jonas, Vadim Migunov, Alberto Eljarrat, Jan Caron, Thomas Aarholt, Stefano Mazzucco, Michael Walls, Tom Slater, Florian Winkler, pquinn dls, Ben Martineau, Gaël Donval, Robert McLeod, Eric R. Hoglund, Ivo Alxneit, Daniel Lundeby, Trond Henninen, Luiz Fernando Zagonel, Andreas Garmannslund, Hyperspy/hyperspy: HyperSpy v1.5.2, Zenodo, 2019, https://doi.org/10.5281/zenodo.3396791.

[22] W.Q. Hong, Extraction of extinction coefficient of weak absorbing thin films from special absorption, J. Phys. Appl. Phys. 22 (1989) 1384–1385, https://doi.org/10.1088/0022-3727/22/9/024.

[23] J. Tauc, Optical properties and electronic structure of amorphous Ge and Si, Mater. Res. Bull. 3 (1968) 37–46, https://doi.org/10.1016/0025-5408(68)90023-8.

[24] E.A. Kraut, R.W. Grant, J.R. Waldrop, S.P. Kowalczyk, Precise determination of the valence-band edge in X-ray photoemission spectra: application to measurement of semiconductor interface potentials, Phys. Rev. Lett. 44 (1980) 1620–1623, https://doi.org/10.1103/PhysRevLett.44.1620.

[25] A. Niemegeers, M. Burgelman, A. De Vos, On the CdS/CuInSe_2 conduction band discontinuity, Appl. Phys. Lett. 67 (1995) 843, https://doi.org/10.1063/1.115523.

[26] C. Platzer-Björkman, J. Kessler, L. Stolt, Analysis of Zn(O,S) films for Cu(In,Ga)Se_2 solar cells, Proc. Est. Acad. Sci. Phys. Math. 52 (2003) 299–307.

[27] J. Lindahl, J. Keller, O. Donzel-Gargand, P. Szaniawski, M. Edoff, T. Törndahl, Deposition temperature induced conduction band changes in zinc tin oxide buffer layers for Cu(In,Ga)Se_2 solar cells, Sol. Energy Mater. Sol. Cell. 144 (2016) 684–690, https://doi.org/10.1016/j.solmat.2015.09.048.

[28] M. Theelen, F. Daume, Stability of Cu(In,Ga)Se_2 solar cells: a literature review, Sol. Energy 133 (2016) 586–627, https://doi.org/10.1016/j.solener.2016.04.010.

[29] I. Repins, S. Glynn, T.J. Silverman, R. Garris, K. Bowers, B. Stevens, L. Mansfield, Large metastability inCu (In,Ga)Se_2 devices: the importance of buffer properties, Prog. Photovoltaics Res. Appl. 27 (2019) 749–759, https://doi.org/10.1002/pip.3145.

[30] A. Ferguson, P. Dippo, D. Kuciauskas, R. Farshchi, J. Bailey, G. Zapalac, D. Poplavskyy, Optical Spectroscopic Probes of Degradation and Metastability in Polycrystalline (Ag,Cu)(In,Ga)Se2 Absorbers, in: IEEE 7th World Conference on Photovoltaic Energy Conversion (WCPEC), Waikoloa Village, HI, 2018, pp. 3918–3922, https://doi.org/10.1109/PVSC.2018.8548226, 2018.

[31] S.M. Sze, K.K. Ng, Physics of Semiconductor Devices, third ed., Wiley-Interscience, Hoboken, N.J, 2007.